Annales
Geophysicae

Open Access

An investigation of the ionospheric F region near the EIA crest in India using OI 777.4 and 630.0 nm nightglow observations

Navin Parihar[1], **Sandro Maria Radicella**[2], **Bruno Nava**[2], **Yenca Olivia Migoya-Orue**[2], **Prabhakar Tiwari**[3], and **Rajesh Singh**[3]

[1]Equatorial Geophysical Research Laboratory, Indian Institute of Geomagnetism, Tirunelveli 627 011, India
[2]The Abdus Salam International Centre for Theoretical Physics, Strada Costiera 11, 34151 Trieste, Italy
[3]Dr. K. S. Krishnan Geomagnetic Research Laboratory, Indian Institute of Geomagnetism, Allahabad 221 505, India

Correspondence: Navin Parihar (navindeparihar@gmail.com)

Abstract. Simultaneous observations of OI 777.4 and OI 630.0 nm nightglow emissions were carried at a low-latitude station, Allahabad (25.5° N, 81.9° E; geomag. lat. $\sim 16.30°$ N), located near the crest of the Appleton anomaly in India during September–December 2009. This report attempts to study the F region of ionosphere using airglow-derived parameters. Using an empirical approach put forward by Makela et al. (2001), firstly, we propose a novel technique to calibrate OI 777.4 and 630.0 nm emission intensities using Constellation Observing System for Meteorology, Ionosphere, and Climate/Formosa Satellite Mission 3 (COSMIC/FORMOSAT-3) electron density profiles. Next, the electron density maximum (Nm) and its height (hmF2) of the F layer have been derived from the information of two calibrated intensities. Nocturnal variation of Nm showed the signatures of the retreat of the equatorial ionization anomaly (EIA) and the midnight temperature maximum (MTM) phenomenon that are usually observed in the equatorial and low-latitude ionosphere. Signatures of gravity waves with time periods in the range of 0.7–3.0 h were also seen in Nm and hmF2 variations. Sample Nm and hmF2 maps have also been generated to show the usefulness of this technique in studying ionospheric processes.

1 Introduction

Ground-based airglow observations have been successfully used to derive physical parameters of the emitting region. Firstly, emission intensities are monitored using ground-based photometers or imaging systems, and then different parameters are derived from their intensity information. Examples are atomic oxygen density (Lednyts'kyy et al., 2014; Russell et al., 2005), vertical transport (Broadfoot and Gardner, 2001; Hays et al., 2003), mesospheric temperatures (Innis et al., 2001; Scheer and Reisin, 2007; Holmen et al., 2014; Parihar et al., 2017, and references cited therein), mesospheric winds (Lloyd et al., 1990), density and pressure (Takahashi et al., 2004), thermospheric temperatures and wind velocities (Cocks, 1983; Vila et al., 1998; Ford et al., 2006, 2008; Nakamura et al., 2017), F region peak electron density and its height (Sahai et al., 1981; Makela et al., 2001), F region zonal drifts (Yao and Makela, 2007), etc. Often the derived parameters are then utilized to understand the behaviour of the emitting region, mainly its chemistry, dynamics and electrodynamics (Semenov, 1988; Fagundes et al., 2001; Makela et al., 2001, 2004; Shiokawa et al., 2003; Scheer and Reisin, 2007; Ford et al., 2008; López-González et al., 2009; Parihar et al., 2013; Holmen et al., 2014). Other ground-based techniques include lidars and radars; however, airglow experiments remain a favourite due to their well-established simplicity, cost-effectiveness and capability for continuous operation on a longer timescale (Ford et al., 2008; Espy et al., 2011; Holmen et al., 2014; Scheer and Reisin, 2007). An important limitation of airglow measurements is that studies are limited to night-time and greatly depend on sky observing conditions.

In the context of the F-region studies, simultaneous measurements of OI 777.4 and 630.0 nm emissions have been successfully used to derive Nm and hmF2 (Makela et al.,

2001) (where Nm and hmF2 are the F region peak electron density and its height, respectively). Theoretical foundation for deriving the electron density and corresponding peak using simultaneous measurements of two airglow emissions from the F region was laid by Tinsley and Bittencourt (1975). Using a correlative study of airglow measurements with the ionosonde measured parameters, Sahai et al. (1981) noted good correlation between (i) $\sqrt{I_{7774}}$ and Nm, and (ii) $(\sqrt{I_{7774}})/I_{6300}$ and hmF2, where I_{7774} and I_{6300} are OI 777.4 and 630.0 nm emission intensities, respectively. Makela et al. (2001) subsequently improved this technique, and formulated empirical equations for estimating Nm and hmF2 from two emission intensities. Makela et al. (2001) utilized this technique to generate spatial (topographic) maps of the F region of ionosphere using all-sky imaging observations of these two emissions, and presented two case studies. A topographic map of the ionosphere features the 3-D representation of electron density and height of the F region of the ionosphere. The potential usefulness of this technique has not been explored since then. Again, limited reports exist in literature that feature simultaneous measurements of these two emissions (Sahai et al., 1981; Makela et al., 2001; Abalde et al., 2004). Sahai et al. (1981) and Makela et al. (2001) linked two emission intensities to the F region parameters Nm and hmF2, while Abalde et al. (2004) estimated the vertical drift velocities from such measurements. Motivated by this, firstly, we attempt to derive Nm and hmF2 from simultaneous measurements of these two emission intensities over Allahabad (25.5° N, 81.9° E), India, on 14 nights during September–December 2009, and then study the signatures of the equatorial ionization anomaly (EIA), the midnight temperature maximum (MTM) phenomenon and gravity waves (GWs) observed in the F region using these limited data.

Firstly, an overview of the underlying theory behind Nm and hmF2 estimation from emission intensities, assumptions therein and its limitations have been presented. Next, OI 777.4 and 630.0 nm emission raw intensities have been calibrated to Rayleigh units using empirical equations of Makela et al. (2001), and with inputs from Constellation Observing System for Meteorology, Ionosphere, and Climate/Formosa Satellite Mission 3 (COSMIC/FORMOSAT-3) electron density profiles. Nm and hmF2 have then been derived from two calibrated intensities, and their nocturnal behaviour has been investigated for the signatures of EIA, MTM and GWs. Sample Nm and hmF2 maps have also been generated to illustrate the usefulness of this technique in understanding ionospheric processes like equatorial plasma bubbles. Earlier, Mukherjee et al. (2000, 2006) reported the nocturnal behaviour of the low-latitude ionosphere over Kolhapur (17° N), India, using OI 630.0 nm measurements. However, to the best of our knowledge, the observations of OI 777.4 nm emission or its simultaneous measurements with OI 630.0 nm emission over India have not been reported.

2 Nm and hmF2 measurements: underlying theory, assumptions and limitations

The basis of determining Nm and hmF2 lies in the excitation mechanisms of OI 777.4 and 630.0 nm emissions (Sahai et al., 1981; Makela et al., 2001). During the night-time, the following recombination reaction involving the O^+ ion and electron is the principal source of OI 777.4 nm emission (Tinsley et al., 1973):

$$O^+ + e \rightarrow O(^5P). \tag{1}$$

Ignoring the contribution of the ion–ion recombination mechanism to OI 777.4 nm emission (Tinsley et al., 1973), its intensity (I_{7774}) depends upon the product of O^+ ion concentration, $[O^+]$, and electron density, n_e. Assuming the quasi-neutral ionospheric plasma to be mainly composed of O^+ ions and electrons, its intensity can be seen depends on $n_e(h)^2$, where $n_e(h)$ is the electron density at height h. Now $n_e(h)$ is related with Nm through the well-known Chapman's function (Tinsley et al., 1973). After detailed numerical computation and correlative study involving the Mass Spectrometer Incoherent Scatter (MSIS-86) model (Hedin, 1987) and International Reference Ionosphere 1995 (IRI-95) model (Bilitza, 1997), Makela et al. (2001) arrived at the following empirical equation:

$$N_m = [3.06 \times \sqrt{I_{7774}} - 1.11] \times 10^{11}, \tag{2}$$

where N_m is in m^{-3}. Subsequently, the critical frequency of the F2 layer, foF2, in MHz, can be estimated from Nm (in m^{-3}) using the following expression (Tinsley et al., 1973):

$$N_m = 1.24 \times 10^{10} \times (foF2)^2. \tag{3}$$

Next, the determination of hmF2 is based on the chemistry of OI 630.0 nm emission. During night-time, this emission feature is primarily due to the following dissociative recombination reaction involving an O_2^+ ion and an electron (Link and Cogger, 1988):

$$O_2^+ + e \rightarrow O^*(^1D) + O. \tag{4}$$

However, the formation of the O_2^+ ion is due to charge exchange between molecular oxygen, O_2, and the O^+ ion as

$$O^+ + O_2 \rightarrow O_2^+ + O. \tag{5}$$

Thus, the production of O_2^+ strongly depends upon both the O_2 density and the height of the F layer. Because of this $[O_2]$ association, the intensity of OI 630.0 nm (I_{6300}) depends upon the height of the F layer apart from the electron density. Link and Cogger (1988) found that the intensity of this emission depends on $[N_2]$ and $[O_2]$ of the neutral atmosphere. As the density of the neutral atmosphere decreases exponentially with height around the OI 630.0 nm emission altitude, such dependency is also likely to exist between its

intensity and the height of the F layer. Using the emission rate of OI 630.0 nm nightglow given by Link and Cogger (1988), and adopting the approach of Tinsley and Bittencourt (1975) and Sahai et al. (1981), Makela et al. (2001) arrived at the following expression relating the $\sqrt{I_{7774}}/I_{6300}$ ratio with the height of the F layer (in km):

$$hmF2 = e^{0.171 \times \ln\left[\sqrt{I_{7774}}/I_{6300}\right] + 6.43}. \tag{6}$$

This expression has been used to determine the height of the peak of electron density in the present study.

3 Experimental set-up and data

Simultaneous observations of OI 777.4 and 630.0 nm nightglow emissions were carried out at a low-latitude station, Allahabad (25.5° N, 81.9° E; geomag. lat. $\sim$ 16.30° N), India, located near the crest of the ionization anomaly, during September–December 2009. An all-sky imager (Keo Scientific Ltd., Canada) was operated to monitor the nightglow emissions under clear-sky conditions and around the new moon period. Parihar and Taori (2015) have described this imaging system in detail. The interference filters, with a bandwidth of $\sim$ 2 nm and transparency in the 66–77 % range, were utilized to monitor the OI 777.4, 630.0 and background emission at 530 nm, with an exposure time of 90 s. The signal-to-noise ratio for these settings of imaging was better than 22.6 dB. The observations of OI 557.7 nm and OH broadband emissions were also made. The time duration of each sequential observation was 9 min. On each night, a flat-field image was taken during the start of imaging observations, and subsequent images recorded by the imaging system were divided by this flat-field image to approximately account for artefacts due to the van Rhijn effect and pixel-to-pixel non-uniformity of the charge coupled device (CCD) detector. Using known astral positions, the location of the zenith was identified in airglow images. For simplicity, average intensity of a square bin (corresponding to a field of view of $\sim$ 4° along the zenith at an altitude of 250 km) in imaging observations has been considered. Such a consideration will help in comparing results of the electron density and height measurements with those of ionosonde and FORMOSAT-3/COSMIC observations. Using this intensity and timestamp information of each image, an intensity time series was generated and used in this study. The details of this technique are discussed elsewhere (Parihar and Taori, 2015; Parihar et al., 2017).

Assuming that the transmission of filters and sensitivity of the CCD detector is the main source of experimental error, the uncertainty in the intensity measurements is estimated to be $\sim$ 8 %. Using this information, the errors in airglow-derived Nm, hmF2 and foF2 have been estimated and the derived quantities are uncertain by $1.68 \times 10^{10}\,m^{-3}$, 5.56 km and 0.14 MHz, respectively. Nightglow observations were severely affected by the presence of clouds during September, while the foggy weather conditions affected observations during November–December. Consequently, good-quality data of 14 nights only were available for a meaningful study. Mostly, the duration of continuous observation on each night was typically 6–8 h, and the Nm/foF2/hmF2 dataset consisted of $\sim$ 40–60 measurements. On these nights, the geomagnetic activity index, Ap, lay between 0 and 13 units and the F10.7 cm solar flux varied in the range of 69–82 units (http://isgi.unistra.fr; last access: 29 May 2018, www.swpc.noaa.gov; last access: 29 May 2018). The majority of the nights (about nine) fell in the category of quiet nights, with 14 October being the quietest one. The most geomagnetically disturbed one was 22 October.

COSMIC/FORMOSAT-3 data: COSMIC/FORMOSAT-3 is a joint Taiwanese–US mission that utilizes a radio occultation (RO) technique to determine physical parameters like temperature, pressure, water vapour, electron density, total electron content and the S4 scintillation index. (Anthes et al., 2008). The COSMIC electron density data were downloaded from the COSMIC Data Analysis and Archive Center (CDAAC, http://cdaac-www.cosmic.ucar.edu/cdaac/index.html; last access: 29 May 2018).

Ionosonde data: A state-of-the-art Canadian Advanced Digital Ionosonde (CADI) system is permanently installed at Allahabad and carries out the vertical soundings in the 1–20 MHz frequency range. Due to some technical issues associated with CADI, only a few hours of ionosonde data were available on 16 September 2009. Ionograms were recorded at 5 min intervals, and were scaled manually to accurately obtain foF2 (the critical frequency of the F2 layer) and hpF2 (the virtual height at 0.834 of foF2 determined by a parabolic approximation) (Piggott and Rawer, 1972).

4 Calibration of OI 777.4 and 630.0 nm intensities

Nm and hmF2 derivation using the empirical expressions (2) and (6) utilize calibrated emission intensities in Rayleigh. In our case, absolute calibration of emission intensities was not possible due to the lack of a standard low brightness source. In a similar situation, Makela et al. (2001) utilized the collocated radar measurements of the electron density and height to calibrate OI 777.4 and 630.0 nm intensities in their investigations using expressions (2) and (6). "Calibration term" is a factor that converts the observed inte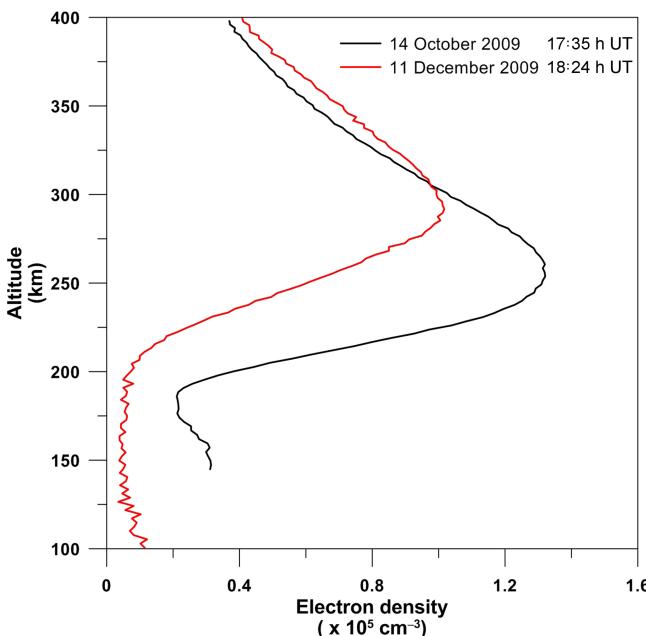nsity of an emission feature from arbitrary units to Rayleigh units. Similarly herein, the coincidental COSMIC electron density profiles in the latitude–longitude grid of 5° $\times$ 5° centred over Allahabad have been used to calibrate the two intensities. Such an approach is based on the comparison of the electron density profiles derived from COSMIC RO measurements and ground-based ionosonde measurements reported recently by Hu et al. (2014) and Limberger et al. (2015). Hu et al. (2014) compared the COSMIC Nm values with

Table 1. Calibration factor of OI 777.4 and 630.0 nm emission intensity inferred using the coincidental COSMIC profiles along with the azimuthal smearing of their tangent point trajectory.

Date	Time (UT)	COSMIC electron density profile information					Inferred calibration factor for observed intensity		
				Spatial spread of COSMIC profile					
		Maximum electron density (Nm) (m^{-3})	Corresponding altitude (hmF2) (km)	Latitude (° N)	Longitude (° E)	Trajectory's azimuth	Closest airglow coincidence time (UT)	OI 777.4 nm	OI 630.0 nm
14.10.2009	1735	1.321×10^{11}	253.8	24.72–27.57	79.41–84.39	32.05–34.75°	1733	5.4×10^{-3}	0.58
11.12.2009	1824	1.017×10^{11}	291.8	25.05–26.38	79.42–84.37	00.08–02.37°	1827	3.0×10^{-3}	0.15

Figure 1. Coincidental COSMIC electron density profiles in the latitude–longitude grid of 5° × 5° centred over Allahabad (25.5° N, 81.9° E) on 14 October and 11 December 2009.

Figure 2. Nocturnal variation of the calibrated intensity of OI 777.4 and 630.0 nm emissions on 24 October 2009 (20:00–06:00).

the ionosonde measurements at four stations over China spread in the 18–54° N latitude range and noted correlation of 0.90 or more amongst the two measurements. Limberger et al. (2015) studied the Nm/hmF2 measurements inferred from the COSMIC/FORMOSAT-3 electron density profiles and performed a global comparison with the ionosonde measurements from 2006 to 2014. These authors found a correlation coefficient of 0.94 and 0.76 between the COSMIC and ionosonde measurements for Nm and hmF2, respectively, in the geomagnetic latitude range of 0–20°. Coinciding with our experiments, two COSMIC coincidences were available in the 5° × 5° latitude–longitude grid over Allahabad – one each on 14 October and 11 December 2009 (hereafter CP1 and CP2, respectively). These COSMIC electron density profiles were checked for data quality and are shown in Fig. 1. The azimuthal smearing of the tangent point trajectory COSMIC profiles CP1 and CP2 is also tabulated in Table 1. Us-
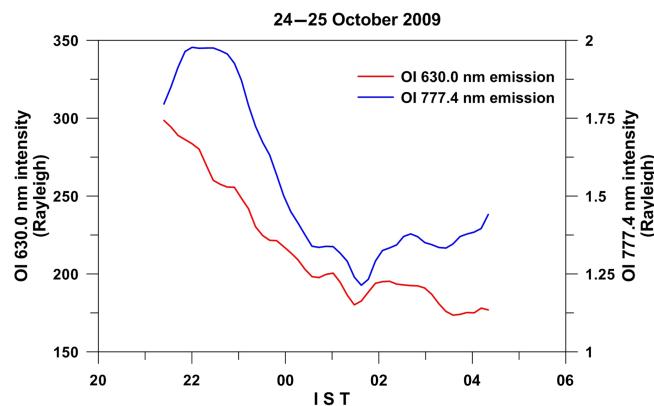
ing Nm and hmF2 information of each COSMIC profile, corresponding OI 777.4 and OI 630.0 nm intensity was estimated using Eqs. (2) and (6), respectively. Using this estimated intensity and the observed one, the calibration term for both emissions was derived. Table 1 summarizes the calibration factors obtained using two COSMIC profiles. Figure 2 presents a typical example of nocturnal variation of two calibrated intensities on 24 October 2009 using CP1 calibration terms. Table 1 clearly indicates dissimilar values of calibration terms inferred from CP1 and CP2 for each emission, thereby making it difficult to infer a suitable calibration factor. Next, a comparison of airglow-derived quantities with coincidental ionosonde measurements from 16 September 2009 was performed to identify the suitable calibration term.

First, two datasets of calibrated intensities corresponding to each set of calibration factors were generated. Next, the critical frequency of the F2 layer (foF2) and the peak height of electron density (hmF2) were derived using Eqs.(2), (3) and (6) from each dataset. For convenience, "Case I" (CP1) refers to the foF2–hmF2 dataset derived from the two emission intensities calibrated using CP1. Similarly, "Case II" (CP2) addresses the ionospheric measurements when the second calibration set inferred from CP2 is used for calibrating intensities. Table 2 summarizes the two sets of the airglow-
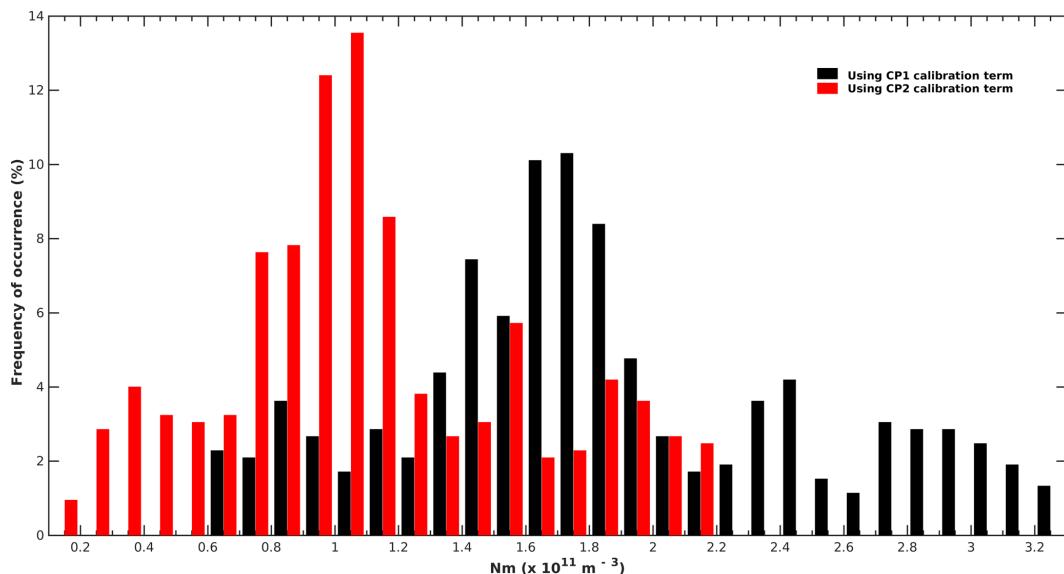
Figure 3. Frequency of occurrence of derived Nm over Allahabad based on 14 nights of data during September–December 2009. Nm values derived from OI 777.4 nm emission intensity using CP1 and CP2 calibration terms are shown by black and red bars, respectively.

Table 2. Comparison of the critical frequency of F2 layer (foF2) and corresponding peak of maximum electron density (hmF2) inferred from OI 777.4 and 630.0 nm emission intensity with the ionosonde measurements (foF2 and hpF2) on 16 September 2009.

Time	Airglow observations				Ionosonde measurements		
	Case I (CP1)		Case II (CP2)				
	foF2 (in MHz)	hmF2 (km)	foF2 (in MHz)	hmF2 (km)	Time	foF2 (in MHz)	hpF2 (km)
24.94	2.73	284.9	1.84	341.0	24.92	2.88	274.9
25.09	2.67	280.7	1.77	336.0	25.17	2.67	266.6
25.24	2.56	277.1	1.65	331.7	25.25	2.75	270.7
25.39	2.71	278.6	1.81	333.5	25.33	2.66	270.7
25.54	2.73	276.9	1.84	331.5	25.50	2.74	268.6
25.69	2.69	274.9	1.79	329.1	25.67	2.65	268.6

derived quantities along with the ionosonde measurements. The closest coincidences in time have been considered for better comparison. It is clear from Table 2 that the CP1 dataset appears to be more realistic and is in better agreement with the ionosonde measurements in comparison to the CP2 dataset. In CP1, hmF2 (height of electron density peak) and hpF2 (virtual height at 0.834 foF2) vary by 10 km or less. Batista et al. (1991) have reported such departures in hmF2 and hpF2 during night-time. On the other hand, the difference between hmF2 and hpF2 is fairly large in CP2. Hence, two intensities calibrated using CP1 calibration terms have been used to derive Nm and hmF2 for studying the behaviour of the F region over Allahabad. Nm and hmF2 derived from two intensities using CP2 calibration terms have also been discussed. Herein, the calibration of intensities strongly depends upon the experimental set-up, exposure times and CCD characteristics that were kept unchanged dur-

ing September–December 2009. Hence, the calibration term is assumed to hold well for the entire data.

5 Observations, results and discussions

5.1 Nm and hmF2 measurements

Figures 3 and Figure 4 present the frequency of occurrence of derived Nm and hmF2, respectively, during September–December 2009. In both figures, black bars represent the F region measurements using the CP1 calibration term, while those in red depict measurements using the CP2 calibration term. Hereafter, Nm values derived using CP1 and CP2 calibrated intensities are termed as Nm^{CP1} and Nm^{CP2}, respectively, while hmF2 values derived using CP1 and CP2 calibration are referred to as $hmF2^{CP1}$ and $hmF2^{CP2}$, respectively. Nm^{CP1} measurements
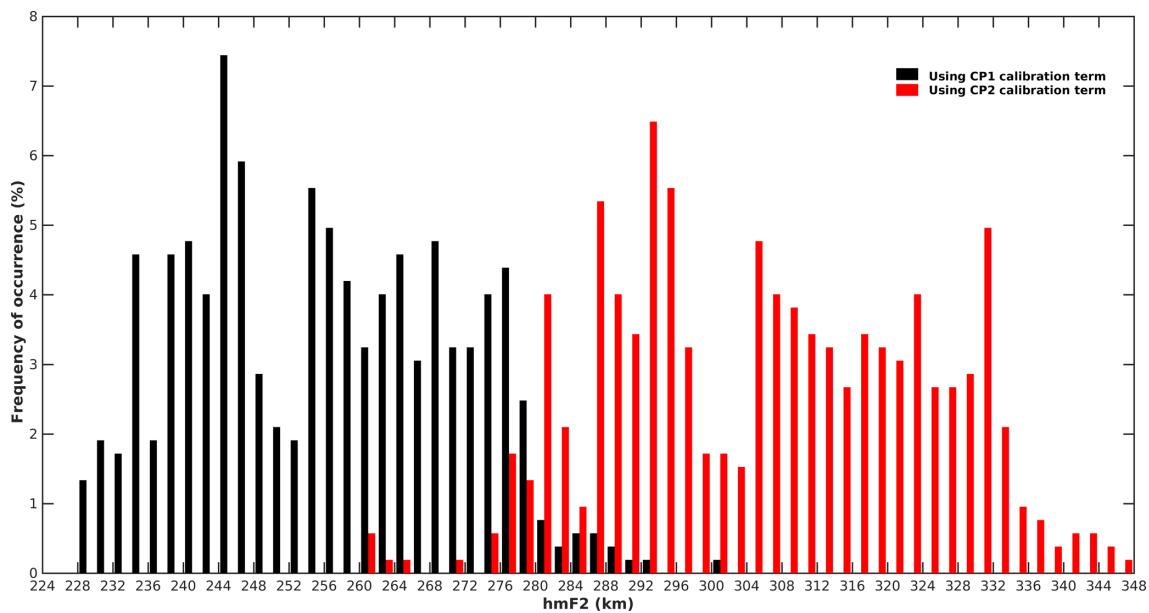
Figure 4. Same as Fig. 3 but for hmF2 derived from the ratio of $\sqrt{I_{7774}}$ and I_{6300}.

are in the range of 0.9–3.2×10^{11} m^{-3}, while Nm^{CP2} values were ~ 0.7–1.0×10^{11} m^{-3} lower than corresponding Nm^{CP1} measurements. Nm^{CP1} was seen to vary in the range of 1.2–2.1×10^{11} m^{-3} in about 59 % of measurements. Nm^{CP2} measurements usually lay in the range of 0.3–1.4×10^{11} m^{-3}. During EIA and MTM events, Nm values were relatively higher, and will be discussed later. A prominent peak in the occurrence of Nm^{CP1} and Nm^{CP2} centred about 1.7×10^{11} m^{-3} and 1.0×10^{11} m^{-3}, respectively, can clearly be seen in Fig. 3. Unlike Nm measurements, derived hmF2 was found to vary in two ranges, and hmF2^{CP1} values were usually 40–60 km lower than corresponding hmF2^{CP2} measurements. These facts can clearly be seen in Fig. 4. Values of hmF2^{CP1} were found to vary between 230 and 260 km in about 60 % of cases, while hmF2^{CP2} values were observed to lie in the range of 278–304 km in about 43 % of measurements. This lower hmF2 spectrum was centred over around 246 and 294 km for CP1 and CP2 calibration. However, the second range of the F-region peak heights was near uniformly spread over 254–276 km for hmF2^{CP1} measurements and over 306–332 km for hmF2^{CP2} measurements. Overall, mean Nm^{CP1} and Nm^{CP2} values are $1.69 \pm 0.18 \times 10^{11}$ and $0.99 \pm 0.14 \times 10^{11}$ m^{-3}, respectively, while mean hmF2^{CP1} and hmF2^{CP2} values are 258.4 ± 8.2 km and 309.3 ± 9.8 km, respectively. Further, foF2 values were estimated from airglow-derived Nm^{CP1} and Nm^{CP2} using Eq. (3) (hereafter, referred to as foF2^{CP1} and foF2^{CP2}, respectively). The foF2^{CP1} measurements were found to swing between 2.1 and 5.1 MHz, while foF2^{CP2} measurements lie in the range of 1.2–4.2 MHz.

Summary of a few earlier reports and our measurements

Ideally a comparison with co-located ionospheric measurements under similar geophysical conditions is a must to assess our measurements. However, due to the lack of such supporting data during our observational period, we looked at NmF2 and hmF2 measurements previously reported by Sethi et al. (2004), Yadav et al. (2010) and Luan et al. (2015) over latitudes relatively close to that of Allahabad. Reports of Sethi et al. (2004) and Yadav et al. (2010) utilized digital ionosonde measurements over India, while that of Luan et al. (2015) was based on COSMIC measurements. Unfortunately, the observational period of these reports was different from that of our measurements. Sethi et al. (2004) studied the behaviour of hmF2 over New Delhi (28.6° N, 77.2° E; geomag. $\sim 19.4°$ N), India, during 2001–2002, which corresponds to the period of high solar activity, whereas Yadav et al. (2010) studied the diurnal and seasonal variation of foF2 and hmF2 over Bhopal (23.2° N, 77.6° E; geomag. lat. $\sim 14.4°$ N), India, during 2007, which was almost the solar minimum period. Luan et al. (2015) studied the behaviour of the EIA using Nm and hmF2 retrieved from the COSMIC database over an extended period from 2007 to 2012, covering low to high solar activity. During pre-midnight hours, Yadav et al. (2010) found the median values of foF2 to vary between ~ 2.9 and 5.4 MHz during the September–October equinox, while we observed foF2^{CP1} and foF2^{CP2} in the range of 3.0–4.4 and 2.1–3.5 MHz, respectively. During the post-midnight hours, these authors observed foF2 in the 2.2–3.0 MHz range, whereas airglow-derived foF2^{CP1} and foF2^{CP2} were in the range of 3.3–4.0 and 2.4–3.1 MHz, respectively. During the passage of the
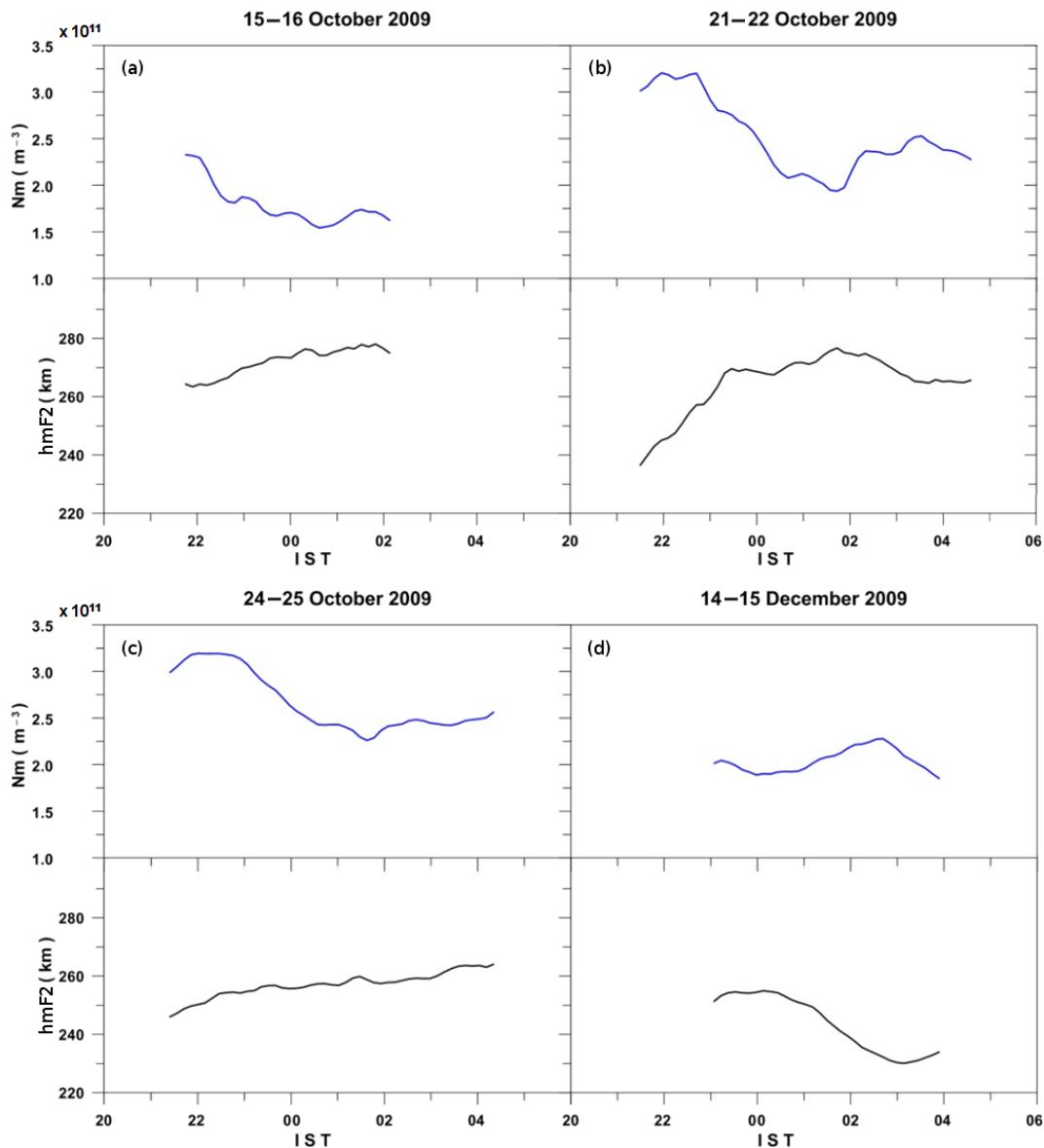
Figure 5. Nocturnal variation of Nm and hmF2 derived using the CP1 calibration term on a few nights in October and December 2009 (20:00–06:00).

crest of the EIA and MTM over Allahabad, comparatively higher values were noted as high as ~ 5.2 and ~ 4.2 Mhz for foF2$^{\text{CP1}}$ and foF2$^{\text{CP2}}$ measurements, respectively. NmF2 maps reported by Luan et al. (2015) indicate Nm values in the range of 2–4×10^{11} m^{-3} near Allahabad at 20:00 LT during the solstice of December 2008. Our airglow-derived Nm$^{\text{CP1}}$ and Nm$^{\text{CP2}}$ values are observed to vary in the range of 1.6–2.0×10^{11} and 0.9–1.3×10^{11} m^{-3}, respectively, during 19:30–20:30.

So far as hmF2 measurements are concerned, Yadav et al. (2010) found hmF2 to vary in the 240–302 km range, whereas derived hmF2$^{\text{CP1}}$ and hmF2$^{\text{CP2}}$ vary in the range of 230–280 and 280–330 km, respectively. Sethi et al. (2004)

observed the median value of hmF2 to vary between 290 and 350 km during the night in the equinoctial months.

5.2 Nocturnal behaviour of Nm: Signatures of EIA and MTM

Typical examples of the airglow-derived Nm and hmF2 of the F layer over Allahabad during October and December 2009 are shown in Fig. 5a–d. Nm and hmF2 are presented in the top and bottom panels, respectively. For simplicity, Nm and hmF2 derived from two intensities using CP1 calibration terms have been presented and discussed herein. Figure 6 presents the variation of Nm and hmF2 on 14 and 22 October (a slightly geomagnetically disturbed day) and
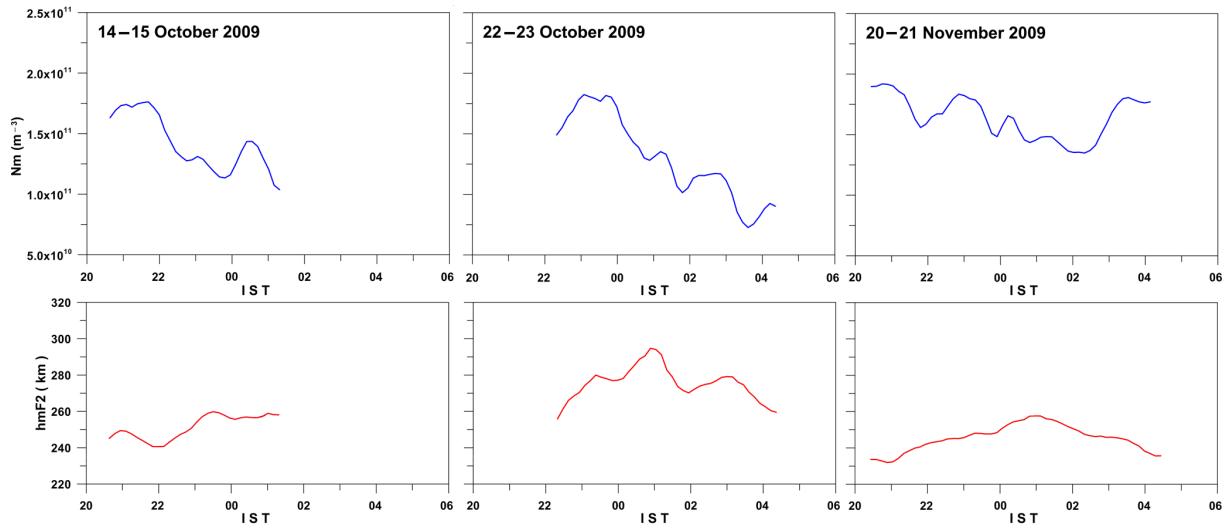
Figure 6. Nocturnal variation of derived Nm and hmF2 on 14 and 22 October (a slightly geomagnetically disturbed day) and 20 November 2009 (20:00–06:00).

20 November. Nocturnal variation of the Nm displayed the common behaviour noted globally at low latitudes (Danilov and Vanina-Dart, 2010; Chakraborty and Hajra, 2009, and references cited therein). On most nights (especially in October), the Nm variations during pre-midnight hours were marked by the signatures of the retreat of the EIA as an elevated peak during 21:00–24:00 (mostly during October). For example, the EIA peak was noted during 21:00–23:00 on 14, 21 and 24 October 2009. On the slightly disturbed nights of 22 October and 20 November, the EIA peak was noted during 22:30–24:00 (about 1–2 later in comparison to its occurrence on the quiet nights; see Fig. 6). During the maximum of EIA on 21 and 24 October, Nm was found to reach $\sim 3.2 \times 10^{11}$ m^{-3}. At Allahabad, with the geomagnetic latitude of $\sim 16.3°$ N, the presence of such peaks corresponding to the EIA is not unusual. The EIA is a well-known feature of the low-latitude ionosphere. The crests in ionization are formed on both sides of the geomagnetic equator by the combined effects of the upward $E \times B$ plasma drift and the ambipolar diffusion along geomagnetic field lines during morning–noon hours, progress towards off-equatorial geomagnetic latitudes of about $\pm 18°$ and retreat towards equator during night-time. EIA development strongly depends on (i) the strength of the eastward electric field and (ii) the transport of ionospheric plasma along the field lines (controlled by the rate of diffusion and neutral winds) (Rastogi and Klobuchar, 1990; Pavlov, 2006; Chakraborty and Hajra, 2009; and references cited therein). Hence, one possible explanation is that a strong upward $E \times B$ drift occurred at the geomagnetic equator that lifted the ionization to higher altitudes, which then diffused to off-equatorial latitudes beyond that of Allahabad. Moreover, these observations of the EIA crests are in the winter months of October–

December; the transequatorial neutral winds blowing across the summer–winter hemisphere might have possibly pushed the EIA to latitudes as high as Allahabad (Luan et al., 2015). Our results on the observations of EIA are in reasonable agreement with some of the earlier reports (Rao and Malhotra, 1964; Rama Rao et al., 1977; Lin et al., 2007; Chakraborty and Hajra, 2009; Zhao et al., 2009). Studies by Rao and Malhotra (1964) on the latitudinal variation of foF2 in the Asian sector suggest that the EIA can persist at least until 02:00 LT at $\sim 30°$ dip latitude. Using 40 MHz radio beacon signals, Rama Rao et al. (1977) investigated diurnal variation of total electron content (TEC) over Waltair (18° N), India, and found a well-defined decrease of the anomaly during 19:00–21:45 LT during the equinox months. A study of time evolution of EIA by Lin et al. (2007) using FORMOSAT-3/COSMIC data of July–August 2006 suggests the presence of a decayed EIA during 19:00–23:00 LT around 15° geomagnetic latitude, with Nm in the $2–5 \times 10^{11}$ m^{-3} range. Using GPS TEC measurements, Chakraborty and Hajra (2009) and Zhao et al. (2009) have investigated the EIA characteristics over Calcutta (23° N), India, during 1978–1990 and in the Asian–Australian sector (50° N–30° S, 95–135° E) during 1996–2004, respectively. Apart from the usual daytime TEC maximum, Chakraborty and Hajra (2009) noted a secondary maximum in TEC variations during 18:00–20:00 IST which were highly correlated with the equatorial electrojet strength. Zhao et al. (2009) observed (i) the EIA crest to appear during 20:00–22:00 LT near 20–22° N latitude during December–February, and (ii) the behaviour of EIA to be more dependent on solar activity near the regions of the anomaly crest. Using a chain of seven ionosonde stations spread in the 10–29° N latitude range in India, Yadav et al. (2013) investigated the latitudinal shifting of the EIA

crest, and found the EIA crest during equinoxes to appear at around 21, 24 and 26° N, respectively, for low, moderate and maximum solar activity of the 19th solar cycle.

Around midnight, Nm was observed to reach its minimum during 00:00–02:00 on most occasions. Beyond 02:00, an additional shallow hump in Nm variations was observed around 03:00. Such behaviour can clearly be seen on 21 October and 14 December (shown in Fig. 5). Such a feature in the thermospheric nightglow measurements has been linked to the midnight pressure bulge/temperature maximum (MTM) phenomenon (Rao and Sastri, 1994; Batista et al., 1997; Mukherjee et al., 2006; Shepherd, 2016; Figueiredo et al., 2017). MTM refers to an unusual large-scale increase in the thermospheric temperatures in the equatorial region around midnight hours due to convergence of (i) eastward zonal wind driven by the day–night differential heating, (ii) upward propagating tides and (iii) in situ thermospheric tides produced by solar extreme ultraviolet associated heating. This convergence reverses the flow of the thermospheric meridional wind from equatorwards towards the poles, thereby pushing plasma to off-equatorial latitudes. This causes an increase in the recombination reaction; hence, there is an enhancement of OI 777.4 and 630 nm emission intensity (Figueiredo et al., 2017, and references cited therein). On 20 November, a sharp ascent of Nm (shown in Fig. 6) as a consequence of the MTM phenomenon is observed; however, its descent appears to be possibly masked by the dawn time enhancement of electron density. During such events, the MTM-associated peak was usually observed around 03:00 IST (as can be seen in Figs. 5 and 6). Studies using Doppler width measurements of OI 630.0 nm nightglow over an equatorial station, Kavalur (12.5° N), India, during 1992–1993 by Rao and Sastri (1994), indicate MTM to occur usually an hour after midnight during winter. Mukherjee et al. (2006) studied the behaviour of OI 630.0 nm nightglow at a low-latitude station, Kolhapur (17° N), India, during December 2002–April 2003 and found the MTM associated peaks to occur mostly during 02:00–03:00 LT. Overall, the behaviour of Nm during the night was characterized by (i) the signatures of the ionization anomaly in the pre-midnight sector, (ii) a minimum around 00:00–02:00 and (iii) a hump as a consequence of the midnight temperature maximum phenomenon beyond 02:00. Sometimes a monotonous decrease of Nm throughout the night was also noted (e.g. on 22 October in Fig. 6).

5.3   Nocturnal behaviour of hmF2

As pointed out earlier, hmF2 was usually observed to vary in two ranges during the night: sometimes between around 230 and 260 km, and otherwise in the range of $\sim$ 250–285 km. For example, hmF2 variations were found to lie in the 230–250 km range on 20 November (shown in Fig. 6). As can be seen in Figs. 5 and 6, hmF2 was generally found to increase during the pre-midnight hours. For example, hmF2

went up from $\sim$ 260 to $\sim$ 279 km on 15 October. On 21 October, a comparatively sharp change in hmF2 (from 230 to 270 km) is seen during 21:30–23:30. On this night, a peak corresponding to the motion of the EIA was observed in 777.4 nm intensity variations during 21:30–23:00. However, its signature was not seen in 630.0 nm intensity variations, which rather showed a decrease. As OI 630.0 nm emission intensity depends on both the electron density and height of the F layer, an increase in the height of F layer is interpreted. hmF2 was found to increase from 236 to 256 km during 21:30–23:00. A similar situation was observed on 24 October (shown in Fig. 2) during 21:30–23:00; however, the height change was less (from 246 to 255 km) in comparison to that observed on 21 October. In the post-midnight sector, hmF2 was found to attain its maximum during 00:00–02:00 and then decrease during the rest of the night. During the occurrence of MTM, the lowering of hmF2 in the $\sim$ 10–20 km range was observed. This can clearly be seen on 21 October, 20 November and 14 December in Figs. 5 and 6. In contrast, Mukherjee et al. (2006) observed a large height decent of the F layer in the $\sim$ 20–60 km range. Overall, hmF2 was found to increase in the pre-midnight hours, attain a maximum around 00:00–02:00 and then decrease beyond 02:00. Nearly similar behaviour of hmF2 has been reported by Sethi et al. (2004). During the night, Sethi et al. (2004) found the minimum of hmF2 at $\sim$ 19:00 LT, an increase thereafter followed by a few shallow peaks around midnight and in the post-midnight hours. Atypical hmF2 variations were also observed, for example, (i) wave-like features on 22 October, (ii) a gradual increase in hmF2 from 245 to 264 km throughout the night on 24 October and (iii) the comparatively large variations in hmF2 (in the 250–300 km range) on the slightly disturbed night in comparison with those observed on quiet and moderate nights (see Fig. 6). Matching with our observations on 24 October, Sethi et al. (2004) observed an increase in hmF2 till pre-sunrise hours at $\sim$ 05:00 LT sometimes, especially during winter and equinox months.

5.4   Signatures of gravity waves in Nm and hmF2 variations

Gravity waves are well known to have a profound influence in the mesosphere–lower thermosphere–ionosphere region. Nocturnal variation of airglow-derived Nm and hmF2 over Allahabad often showed the presence of short-period oscillations, especially around the midnight hours. Such wave-like variations are clearly evident on 15 October (in Fig. 5), 22 October and 20 November (in Fig. 6). A Lomb–Scargle periodogram analysis of Nm and hmF2 time series was performed to estimate these wave periodicities. While estimating the wave periodicities, Nm and hmF2 variations during the presence of EIA and MTM have been excluded. Shown in Fig. 5, Nm variations on 15 October were marked by about a 1.3 h period wave-like feature during 22:30–01:00; however, this wave was not seen in hmF2 variations. An about
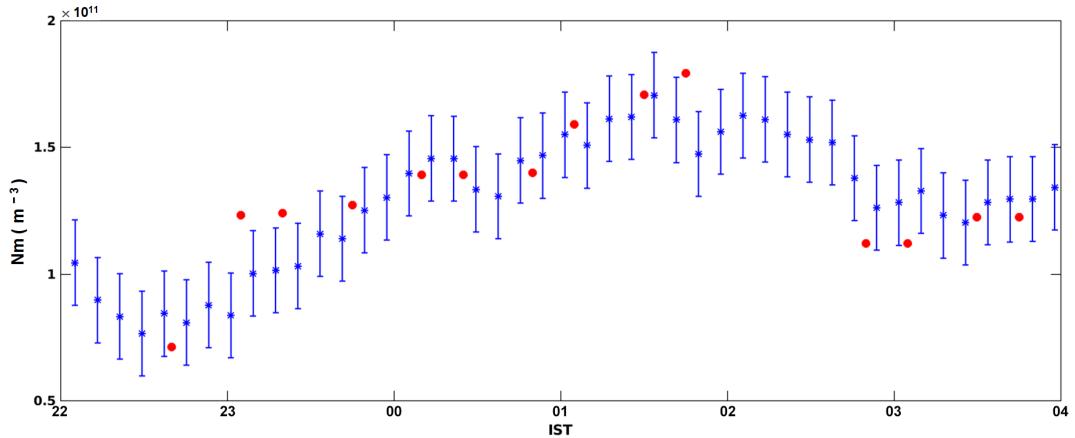
Figure 7. A limited comparison of airglow-derived Nm with ionosonde measurements on 9 January 2016 (22:00–04:00).
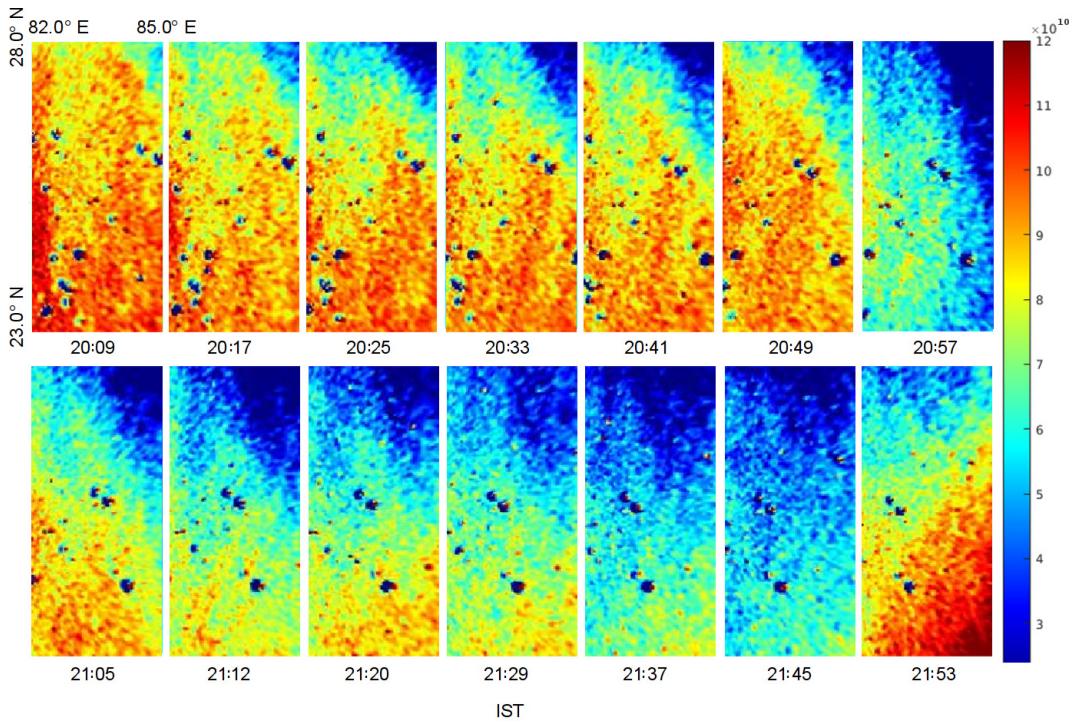

Figure 8. Sequence of airglow-derived Nm maps during 20:00–22:00 IST on 9 January 2016 (Nm is expressed in m^{-3}).

0.8 h period wave feature can be seen in Nm variations during 00:00–02:00 on 22 October (in Fig. 6), while hmF2 variations show the presence of a wave-like oscillation of a period of ~ 2.4 h. On 23 October, 1.5–2.0 h waves were noted in Nm and hmF2 variations. Sometimes similar waves were noted in both Nm and hmF2 variation. For example, a ~ 0.9 h period wave was seen in both Nm and hmF2 variations on 14 October. Overall, a short period (0.7–3.0 h) of wave-like oscillations was noted in Nm and hmF2 variations. Several investigators have reported the presence of such wavelike features in the ionospheric parameters. Using CADI measurements, Klausner et al. (2009) studied the seasonal variation

of gravity waves in the virtual height of the F2 layer at São José dos Campos (23.2° S, 45.9° W), a low-latitude station located under the southern crest of the EIA in Brazil and noted the presence of 30–180 min waves. Ford et al. (2006, 2008) investigated the thermospheric gravity wave activity in temperature and wind velocities inferred from Fabry–Pérot-interferometer-based measurements of OI 630.0 nm emission over northern Scandinavia during 2000–2006, and found the presence of waves with time periods ranging from a few tens of minutes to 8 h. Using all-sky imaging observations of OI 630.0 nm emission, Paulino et al. (2016) studied the presence of thermospheric gravity waves over São João do
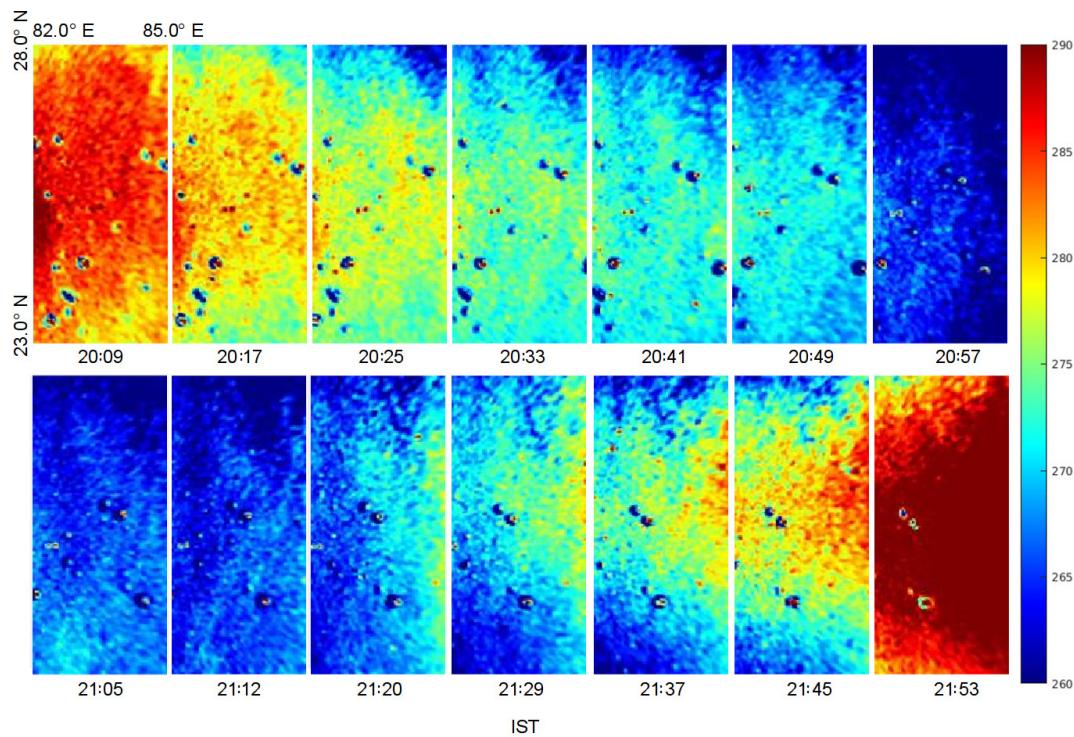
Figure 9. Sequence of airglow-derived hmF2 maps during 20:00–22:00 IST on 9 January 2016 (hmF2 is expressed in km).

Cariri (7.4° S), Brazil, during 2000–2010. Most of the observed waves had time periods of between 5 and 45 min in their study.

5.5 Nm and hmF2 maps over Allahabad

Success of airglow-derived Nm and hmF2 in investigating the behaviour of EIA, MTM and gravity waves motivated us to extend this study to imaging observations. On one occasion (on 9 January 2016), coincidental ionosonde and COSMIC measurements were available along with airglow experiments. A similar calibration approach was adopted using COSMIC data, and Nm and hmF2 were derived from the calibrated intensity. Next, a limited comparison of airglow-derived Nm and hmF2 was done using ionosonde measurements. Figure 7 presents the results of such a comparison for Nm measurements. Airglow and ionosonde measurements are denoted by blue asterisks with error bars and solid red circles, respectively. A reasonable agreement between airglow-derived Nm and ionosonde measurements can be seen. However, disparity between two measurements for hmF2 was noted. Further, we extended this technique to generate Nm and hmF2 maps over a 23–28° N × 82–85° E geographic grid on this night. Figures 8 and 9, respectively, present a sequence of Nm and hmF2 maps during 20:00–22:00. In Nm maps, the signatures of plasma depletions and their drift can clearly be seen. Most depleted regions had an electron density of $\sim 0.3 \times 10^{11}$ m^{-3} or less. However, a decrease in the

height of the F layer from 290 to 260 km till 21:00, and an increase afterwards to 290 km, can be noted in the hmF2 maps.

6 Discussions and future work

Using the empirical equations derived by Makela et al. (2001), Nm and hmF2 have been estimated from OI 777.4 and 630.0 nm emission intensities this report. The study of Makela et al. (2001) is based on the assumptions that (i) ionospheric plasma is mainly composed of O$^+$ ions, (ii) the contribution of the ion–ion recombination mechanism to OI 777.4 nm emission is negligible, (iii) the ionosphere is defined through the well-known Chapman's function, and (iv) the effects of the exospheric temperatures on 777.4 and 630.0 nm intensities are ignored. Authors estimated errors arising from these to be less than 2 and 6 % in Nm and hmF2 measurements, respectively. Further, ions, electrons and neutrals are involved in the complex chemistry in the ionosphere, which results in charge exchange, recombination, dissociative recombination, airglow emissions and quenching of excited states, etc. Altogether these lead to uncertainties in derived quantities, and their estimation is beyond the scope of this present simplified study. Next, due to the lack of a standard low brightness calibration source, intensities were not given in Rayleigh units. An indirect approach was adopted to calibrate them using COSMIC electron density profiles. Coinciding with our experimental period, two such profiles were available that resulted in unusually different sets of cal-

ibration terms. Consequently, two sets of derived Nm and hmF2 were generated. Two Nm measurements were different by $\sim 0.7 \times 10^{11}$ m^{-3}, while a difference of ~ 50 km was seen in two hmF2 measurements. Clearly, a strong dependence of derived Nm on the calibration terms used can be seen and this influences the accuracy of measurements. In terms of temporal coincidence, COSMIC coincidence observed on 14 October was comparatively closer (~ 1 min) to airglow measurements than that observed on 11 December. However, coincidence observed on 11 December was better in terms of spatial coincidence and latitudinal smearing. On 14 October, geographic coordinates of the F-region peak inferred from COSMIC profile were 27.2° N, 80.1° E, while they were 25.7° N, 81.7° E on 11 December. A crucial limitation of this study is that the data are limited to a few nights. The imager was operated during 15 September–15 December 2009; however, due to unfavourable sky conditions, limited data of only 14 nights were available. Next, two COSMIC coincidences were noted coinciding with these observations (listed in Table 1). Each of them yielded a different set of calibration terms; hence, two sets of derived Nm and hmF2 have been discussed in the results. The next period of observation was during 2015 and 2016; however, one COSMIC coincidence was observed on 09 January 2016. The few coincidental cases limit us in inferring a suitable set of calibration terms. An extensive coincidental database of airglow, ionosonde and COSMIC measurements shall be employed in future to validate the trustworthiness of this empirical calibration technique, and to achieve more accuracy in derived Nm and hmF2.

Makela et al. (2001) utilized this technique over an area of 1000×1000 km, centred over Arecibo in Puerto Rico. Unlike them, we have focussed on a limited portion of sky over the zenith. As stated earlier, airglow-observing conditions over Allahabad during 2009 were not very favourable, and all-sky images suffered from light contamination in an annular region near the edges and being minimized radially inward. As Nm and hmF2 measurements greatly depend upon intensity information, we restricted our study to a limited field of view over the zenith. In their study, Sahai et al. (1981) utilized OI 777.4 and 630.0 nm emission intensities measured using photometers with a narrow field of view (3–5°) (similar to the field of view of our sample location), and found good correlations between (i) $(I_{7774})^{1/2}$ and Nm, and (ii) the ratio $(I_{7774})^{1/2}/(I_{6300})$ and hmF2. Furthermore, the electrodynamical features, viz. EIA, MTM and gravity waves (0.7–3.0 h period), discussed herein are large-scale processes (beyond the limited coverage of our imager's field of view of $\sim 140°$). Thus, we believe that the variations observed over the zenith fairly represent the general behaviour of the ionosphere within the limited field of view of the imager. Such a choice further facilitated us in calibrating the intensities using COSMIC electron density profiles. On one occasion (9 January 2016) when good quality all-sky imaging data were available along with the coincidental COSMIC electron density profile for intensity calibration, we were successful in generating Nm and hmF2 maps.

7 Conclusions

This study is an attempt to investigate the behaviour of the F region from an airglow perspective. Simultaneous measurements of OI 777.4 and 630.0 nm nightglow emissions were carried out at Allahabad (26° N), India, during September–December 2009. Using the empirical approach of Makela et al. (2001), two airglow intensities were calibrated to Rayleigh units with the help of COSMIC electron density profiles. Next, the characteristics of the F region, viz. Nm and hmF2, have been derived using airglow measurements. Initial results obtained herein appear to be promising with regards to Nm and hmF2 measurements when airglow intensities are accurately calibrated using COSMIC electron density profiles. Nocturnal variations of Nm and hmF2 were used to study the F region on a limited number of nights. Signatures of the retreat of EIA and MTM, commonly observed in the equatorial and low-latitude ionosphere, were noted in Nm variations. Nocturnal behaviour of hmF2 was similar to that reported earlier by Sethi et al. (2004). Wave-like oscillations with periodicities in the range of 0.7–3.0 h were seen in Nm and hmF2 variations. A severe limitation of this study is the limited airglow data. We plan to extend this study to a larger database so as to achieve more accuracy in Nm and hmF2 measurements and substantiate their use to understand the electrodynamics of the equatorial and low-latitude ionosphere from an airglow perspective.

References

Abalde, J. R., Fagundes, P. R., Sahai, Y., Pillat, V. G., Pimenta, A. A., and Bittencourt, J. A.: Height-resolved ionospheric drifts at low latitudes from simultaneous OI 777.4 nm and OI 630.0 nm imaging observations, J. Geophys. Res., 109, A11308, https://doi.org/10.1029/2004JA010560, 2004.

Anthes, R. A., Ector, D., Hunt, D. C., Kuo, Y-H., Rocken, C., Schreiner, W. S., Sokolovskiy, S. V., Syndergaard, S., Wee, T-K., Zeng, Z., Bernhardt, P. A., Dymond, K. F., Chen, Y., Liu, H., Manning, K., Randel, W. J., Trenberth, K. E., Cucurull, L., Healy, S. B., Ho, S-P., McCormick, C., Meehan, T. K., Thompson, D. C., and Yen, N. L.: The COSMIC/FORMOSAT-3 Mission: Early Results, B. Am. Meteorol. Soc., 89, 313–333, https://doi.org/10.1175/BAMS-89-3-313, 2008.

Batista, I. S., de Paula, E. R., Abdu, M. A., and Trivedi, N. B.: Ionospheric effects of the March 13, 1989 magnetic storm at low and equatorial latitudes, J. Geophys. Res., 96, 13943–13952, 1991.

Batista, I. S., Sastri, J. H., deMedeiros, R. T., and Abdu, M. A.: Nighttime thermospheric meridional winds at Cachoeira Paulista (23° S, 45° W): Evidence for effects of the equatorial midnight pressure bulge, J. Geophys. Res., 102, 20059–20062, https://doi.org/10.1029/97JA01387, 1997.

Bilitza, D.: International reference ionosphere-status 1995/96, Adv. Space Res., 20, 1751–1754, https://doi.org/10.1016/S0273-1177(97)00584-X, 1997.

Broadfoot, A. L. and Gardner, J. A.: Hyperspectral imaging of the night airglow layer from the shuttle: A study of temporal variability, J. Geophys. Res., 106, 24795–24812, 2001.

Chakraborty, S. K. and Hajra, R.: Electrojet control of ambient ionization near the crest of the equatorial anomaly in the Indian zone, Ann. Geophys., 27, 93–105, https://doi.org/10.5194/angeo-27-93-2009, 2009.

Cocks, T. D.: Dual Fabry-Perot spectrometer measurements of daytime thermospheric temperature and wind velocity – Data analysis procedures, Appl. Optics, 22, 726–732, https://doi.org/10.1364/AO.22.000726, 1983.

Danilov, A. D. and Vanina-Dart, L. B.: Behavior of foF2 and hmF2 after sunset, Geomagn. Aeronomy, 50, 796–803, https://doi.org/10.1134/S0016793210060113, 2010.

Espy, P. J., Ochoa Fernández, S., Forkman, P., Murtagh, D., and Stegman, J.: The role of the QBO in the inter-hemispheric coupling of summer mesospheric temperatures, Atmos. Chem. Phys., 11, 495–502, https://doi.org/10.5194/acp-11-495-2011, 2011.

Fagundes, P. R., Sahai, Y., and Bittencourt, J. A.: Thermospheric zonal temperature gradients observed at low latitudes, Ann. Geophys., 19, 1133–1139, https://doi.org/10.5194/angeo-19-1133-2001, 2001.

Figueiredo, C. A. O. B., Buriti, R. A., Paulino, I., Meriwether, J. W., Makela, J. J., Batista, I. S., Barros, D., and Medeiros, A.

F.: Effects of the midnight temperature maximum observed in the thermosphere–ionosphere over the northeast of Brazil, Ann. Geophys., 35, 953–963, https://doi.org/10.5194/angeo-35-953-2017, 2017.

Ford, E. A. K., Aruliah, A. L., Griffin, E. M., and McWhirter, I.: Thermospheric gravity waves in Fabry-Perot Interferometer measurements of the 630.0 nm OI line, Ann. Geophys., 24, 555–566, https://doi.org/10.5194/angeo-24-555-2006, 2006.

Ford, E. A. K., Aruliah, A. L., Griffin, E. M., and McWhirter, I.: Statistical analysis of thermospheric gravity waves from Fabry-Perot Interferometer measurements of atomic oxygen, Ann. Geophys., 26, 29–45, https://doi.org/10.5194/angeo-26-29-2008, 2008.

Hays, P. B., Kafkalidis, J. F., Skinner, W. R., and Roble, R. G.: A global view of the molecular oxygen night airglow, J. Geophys. Res., 108, D204646, https://doi.org/10.1029/2003JD003400, 2003.

Hedin, A. E.: MSIS-86 Thermospheric Model, J. Geophys. Res., 92, 4649–4662, https://doi.org/10.1029/JA092iA0p04649, 1987.

Holmen, S. E., Dyrland, M. E., and Sigernes, F.: Long-term trends and the effect of solar cycle variations on mesospheric winter temperatures over Longyearbyen, Svalbard (78° N), J. Geophys. Res., 119, 6596–6608, https://doi.org/10.1002/2013JD021195, 2014.

Hu, L., Ning, B., Liu, L., Zhao, B., Li, G., Wu, B., Huang, Z., Hao, X., Chang, S., and Wu, Z.: Validation of COSMIC ionospheric peak parameters by the measurements of an ionosonde chain in China, Ann. Geophys., 32, 1311–1319, https://doi.org/10.5194/angeo-32-1311-2014, 2014.

Innis, J. L., Phillips, F. A., Burns, G. B., Greet, P. A., French, W. J. R., and Dyson, P. L.: Mesospheric temperatures from observations of the hydroxyl (6–2) emission above Davis, Antarctica: A comparison of rotational and Doppler measurements, Ann. Geophys., 19, 359–365, https://doi.org/10.5194/angeo-19-359-2001, 2001.

Klausner, V., Fagundes, P. R., Sahai, Y., Wrasse, C. M., Pillat, V. G., and Becker-Guedes, F.: Observations of GW/TID oscillations in the F2 layer at low latitude during high and low solar activity, geomagnetic quiet and disturbed periods, J. Geophys. Res., 114, A02313, https://doi.org/10.1029/2008JA013448, 2009.

Lednyts'kyy, O., von Savigny, C., Eichmann, K.-U., and Mlynczak, M. G.: Atomic oxygen retrievals in the MLT region from SCIAMACHY nightglow limb measurements, Atmos. Meas. Tech., 8, 1021–1041, https://doi.org/10.5194/amt-8-1021-2015, 2015.

Limberger, M., Hernández-Pajares, M., Aragón-Ángel, A., Altadill, D., and Dettering, D.: Long-term comparison of the ionospheric F2 layer electron density peak derived from ionosonde data and Formosat-3/COSMIC occultations, J. Space Weather Spac., 5, 1–13, https://doi.org/10.1051/swsc/2015023, 2015.

Lin, C. H., Liu, J. Y., Fang, T. W., Chang, P. Y., Tsai, H. F., Chen, C. H., and Hsiao, C. C.: Motions of the equatorial ionization anomaly crests imaged by FORMOSAT-3/COSMIC, Geophys. Res. Lett., 34, L19101, https://doi.org/10.1029/2007GL030741, 2007.

Link, R. and Cogger, L. L.: A reexamination of the O I 6300-Å nightglow, J. Geophys. Res., 93, 9883–9892, https://doi.org/10.1029/JA093iA09p09883, 1988.

Lloyd, N., Manson, A. H., McEwen, D. J., and Meek, C. E.: A comparison of middle atmospheric dynamics at Saskatoon (52° N, 107° W) as measured by a medium-frequency radar and

a Fabry-Perot interferometer, J. Geophys. Res., 95, 7653–7660, https://doi.org/10.1029/JD095iD06p07653, 1990.

López-González, M. J., Rodríguez, E., García-Comas, M., Costa, V., Shepherd, M. G., Shepherd, G. G., Aushev, V. M., and Sargoytchev, S.: Climatology of planetary wave type oscillations with periods of 2–20 days derived from O$_2$ atmospheric and OH(6–2) airglow observations at mid-latitude with SATI, Ann. Geophys., 27, 3645–3662, https://doi.org/10.5194/angeo-27-3645-2009, 2009.

Luan, X., Wang, P., Dou, X., and Liu, Y. C.-M.: Interhemispheric asymmetry of the equatorial ionization anomaly in solstices observed by COSMIC during 2007–2012, J. Geophys. Res., 120, 3059–3073, https://doi.org/10.1002/2014JA020820, 2015.

Makela, J. J., Kelley, M. C., González, S. A., Aponte, N., and McCoy, R. P.: Ionospheric topography maps using multiple-wavelength all-sky images, J. Geophys. Res., 106, 29161–29174, https://doi.org/10.1029/2000JA000449, 2001.

Makela, J. J., Ledvina, B. M., Kelley, M. C., and Kintner, P. M.: Analysis of the seasonal variations of equatorial plasma bubble occurrence observed from Haleakala, Hawaii, Ann. Geophys., 22, 3109–3121, https://doi.org/10.5194/angeo-22-3109-2004, 2004.

Mukherjee, G. K., Carlo, L., and Mahajan, S. H.: 630 nm nightglow observations from 17° N latitude, Earth Planet. Space, 52, 105–110, https://doi.org/10.1186/BF03351618, 2000.

Mukherjee, G. K., Parihar, N., Niranjan, K., and Manju, G.: Signature of midnight temperature maximum (MTM) using OI 630 nm airglow, Indian J. Radio Space Phys., 35, 14–21, 2006.

Nakamura, Y., Shiokawa, K., Otsuka, Y., Oyama, S., Nozawa, S., Komolmis, T., Komonjida, S., Neudegg, D., Yuile, C., Meriwether, J., Shinagawa, H., and Jin, H.: Measurement of thermospheric temperatures using OMTI Fabry-Perot interferometers with 70-mm etalon, Earth Planet. Space, 69, 1–13, https://doi.org/10.1186/s40623-017-0643-1, 2017.

Parihar, N. and Taori, A.: An investigation of long-distance propagation of gravity waves under CAWSES India Phase II Programme, Ann. Geophys., 33, 547–560, https://doi.org/10.5194/angeo-33-547-2015, 2015.

Parihar, N., Taori, A., Gurubaran, S., and Mukherjee, G. K.: Simultaneous measurement of OI 557.7 nm, O$_2$ (0, 1) Atmospheric Band and OH (6, 2) Meinel Band nightglow at Kolhapur (17° N), India, Ann. Geophys., 31, 197–208, https://doi.org/10.5194/angeo-31-197-2013, 2013.

Parihar, N., Singh, D., and Gurubaran, S.: A comparison of ground-based hydroxyl airglow temperatures with SABER/TIMED measurements over 23° N, India, Ann. Geophys., 35, 353–363, https://doi.org/10.5194/angeo-35-353-2017, 2017.

Paulino, I., Medeiros, A. F., Vadas, S. L., Wrasse, C. M., Takahashi, H., Buriti, R. A., Leite, D., Filgueira, S., Bageston, J. V., Sobral, J. H. A., and Gobbi, D.: Periodic waves in the lower thermosphere observed by OI630 nm airglow images, Ann. Geophys., 34, 293–301, https://doi.org/10.5194/angeo-34-293-2016, 2016.

Pavlov, A. V.: The role of the zonal E × B plasma drift in the low-latitude ionosphere at high solar activity near equinox from a new three-dimensional theoretical model, Ann. Geophys., 24, 2553–2572, https://doi.org/10.5194/angeo-24-2553-2006, 2006.

Piggott, W. R. and Rawer, K.: URSI Handbook of Ionogram Interpretation and Reduction, World Data Center A for Solar-Terrestrial Physics, Report UAG-23, 2nd Edn., 1972.

Rama Rao, P. V. S., Srirama Rao, M., and Satyam, M.: Diurnal and seasonal trends in TEC values observed at Waltair, Indian J. Radio Space Phys., 6, 233–235, 1997.

Rao, C. S. R. and Malthotra, P. L.: A study of geomagnetic anomaly during I.G.Y., J. Atmos. Terr. Phys., 26, 1075–1085, 1964.

Rao, H. N. R. and Sastri, J. H.: Characteristics of the equatorial midnight temperature maximum in the Indian sector, Ann. Geophys., 12, 276–278, 1994.

Rastogi, R. G. and Klobuchar, J. A.: Ionospheric electron content within the equatorial F2 layer anomaly belt, J. Geophys. Res., 95, 19045–19052, https://doi.org/10.1029/JA095iA11p19045, 1990.

Russell, J. P., Ward, W. E., Lowe, R. P., Roble, R. G., Shepherd, G. G., and Solheim, B.: Atomic oxygen profiles (80 to 115 km) derived from wind imaging interferometer/upper atmospheric research satellite measurements of the hydroxyl and greenline airglow: local time – latitude dependence, J. Geophys. Res., 110, D15305, https://doi.org/10.1029/2004JD005570, 2005.

Sahai, Y., Bittencourt, J. A., Teixeira, N. R., and Takahashi, H.: Simultaneous observations of OI 7774-Å and forbidden OI 6300-Å emissions and correlative study with ionospheric parameters, J. Geophys. Res., 86, 3657–3660, https://doi.org/10.1029/JA086iA05p03657, 1981.

Scheer, J. and Reisin, E. R.: Is there an influence of short-term solar activity variations on mesopause region airglow?, Adv. Space Res., 39, 1248–1255, 2007.

Semenov, A. I.: Seasonal variations of hydroxyl rotational temperature, Geomagnetizm i Aeronomiia, 28, 333–334, 1988.

Sethi, N. K., Dabas, R. S., and Vohra, V. K.: Diurnal and seasonal variations of hmF2 deduced from digital ionosonde over New Delhi and its comparison with IRI 2001, Ann. Geophys., 22, 453–458, https://doi.org/10.5194/angeo-22-453-2004, 2004.

Shepherd, M. G.: WINDII observations of thermospheric O(1D) nightglow emission rates, temperature, and wind: 1. The northern hemisphere midnight temperature maximum and the wave 4, J. Geophys. Res., 121, 11450–11473, https://doi.org/10.1002/2016JA022703, 2016.

Shiokawa, K., Kadota, T., Otsuka, Y., Ogawa, T., Nakamura, T., and Fukao, S.: A two-channel Fabry-Perot interferometer with thermoelectric-cooled CCD detectors for neutral wind measurement in the upper atmosphere, Earth Planet. Space, 55, 271–275, 2003.

Takahashi, H., Nakamura, T., Shiokawa, K., Tsuda, T., Lima, L. M., and Gobbi, D.: Atmospheric density and pressure inferred from the meteor diffusion coefficient and airglow O$_2$b temperature in the MLT region, Earth Planet. Space, 56, 249–258, 2004.

Tinsley, B. A. and Bittencourt, J. A.: Determination of F region height and peak electron density at night using airglow emissions from atomic oxygen, J. Geophys. Res., 80, 2333–2337, https://doi.org/10.1029/JA080i016p02333, 1975.

Tinsley, B. A., Christensen, A. B., Bittencourt, J., Gouveia, H., Angreji, P. D., and Takahashi, H.: Excitation of oxygen permitted line emissions in the tropical nightglow, J. Geophys. Res., 78, 1174–1186, https://doi.org/10.1029/JA078i007p01174, 1973.

Vila, P., Rees, D., Merrien, P., and Kone, E.: Fabry-Perot interferometer measurements of neutral winds and F2 layer variations at the magnetic equator, Ann. Geophys., 16, 731–737, https://doi.org/10.1007/s00585-998-0731-4, 1998.

Yadav, S., Dabas, R. S., Das, Rupesh M., Upadhayaya, A. K., Sharma, K., and Gwal, A. K.: Diurnal and seasonal variation of

F2-layer ionospheric parameters at equatorial ionization anomaly crest region and their comparison with IRI-2001, Adv. Space Res., 45, 361–367, https://doi.org/10.1016/j.asr.2009.08.018, 2010.

Yao, D. and Makela, J. J.: Analysis of equatorial plasma bubble zonal drift velocities in the Pacific sector by imaging techniques, Ann. Geophys., 25, 701–709, https://doi.org/10.5194/angeo-25-701-2007, 2007.

Zhao, B., Wan, W., Liu, L., and Ren, Z.: Characteristics of the ionospheric total electron content of the equatorial ionization anomaly in the Asian-Australian region during 1996–2004, Ann. Geophys., 27, 3861–3873, https://doi.org/10.5194/angeo-27-3861-2009, 2009.